Chapter 4

ELECTRON INTERACTION WITH HYDRATED DNA MOLECULES

In this chapter, we report computed probabilities of various interaction processes taking place during the collision of electrons with DNA molecules, viz., Adenine, Guanine, Cytosine, Thymine and Uracil in their aqueous phase. We have also found various cross sections for furfural and parabezoquinone (pBQ) compounds and Pentafluoropropionic Acid using SCOP, CSP-ic and 2p-SEM formalism. We have also estimated the dielectric constant (Ɛ) for these molecules. We have also examined various correlation between total cross section (Q_T), target molecular properties (no. of target electron and dipole polarizability, α) and also observed correlation between $Q_{ion}\,(Max)$ with dipole polarizability (α) and dielectric constant (Ɛ).

4.1 Introduction

The application of ionising radiation in the field of medicine is extremely common. It is frequently utilized in the medical field as a therapeutic agent and in the field of radio diagnostics as a probe. Ballistic impact was traditionally thought to be the mechanism that was responsible for the majority of the damage that high-energy incident radiation caused to living tissue. However, secondary species that result from primary ionization are responsible for a significant radiation damage [1]. The majority of the energy is deposited by the primary ionising particles once they enter the biological medium through several collision processes, including excitations and ionizations. Large amounts of secondary electrons are released as a result of this significant energy transfer, and these electrons can interact with a variety of biological substances causing the radiation damage. Among all the living tissues, DNA molecules are thought to be most sensitive to radiations. Exposure of DNA species to radiations result in multiple types of DNA damage [2] through secondary species including electrons.

As primary as well as secondary species induces the radiation damage, it is essential to model their tracks through a biological medium. This makes it possible to anticipate and comprehend the type, location, and severity of cell damage. The route taken by the primary and secondary particles as they move through the medium is depicted by the charged-particle track structures [3]. The entire range of interaction between the primary and secondary species at the level of each atom or molecule, is modelled in these stochastic simulations using the cross-section values. Hence, accurate cross-sections are crucial to the validity of these types of simulations.

Till now a lot of cross-sectional data has been reported for the DNA constituents upon electron impact in their gaseous phase [4–8]. Such cross-sections (CSs) are also available for the condensed phase interaction processes but only for the low energy below 20 eV [9,10]. But aqueous phase of the DNA rather than gaseous or condensed phase, presents more realistic picture, as they are always found covered with the water molecules through hydrogen bonding [11,12]. This has motivated us to take up the study of electron interactions with aqueous DNA constituents. We have computed the ionization CSs (Q_{ion}), inelastic CSs (Q_{inel}), elastic CSs (Q_{el}), and total CSs (Q_T) for all the five DNA constituents, viz. Adenine, Guanine, Thymine, Cytosine and Uracil upon electron collisions by considering their aqueous phase. This is the maiden attempt to investigate the electron induced processes for the aqueous DNA constituents for the energies from ionization threshold of the molecules to 5000 eV.

Tan *et.al.* [13] have reported the Q_{inel} data for the case of DNA in water using dielectric response theory and Penn's approximation for energy range from 20-10000 eV. Recently, Vera *et.al.* [14] and Tan *et.al.* [15] has reported the ionization CSs data for DNA compounds by considering their condensed phase for impact energies from 1-10000 eV and 10-500 eV, respectively. All of them used the theoretical methodology which underlines the concept of dielectric response theory.

Since, to the best of our knowledge no work is available for the aqueous phase of DNA molecules; we have developed a new 2-parameter Semi-empirical method (2p-SEM) for computing the Q_T and Q_{el}.

2-furaldehyde or furfural ($C_5H_4O_2$) is an essential component of green chemistry, as well as in the petroleum, agrochemicals, pharmaceuticals, and plastics [16]. Furthermore, it has been recognized as a crucial base chemical [17,18] for the commercialization of bio-refineries. To provide a greater yield of biofuel conversion, biomass is first treated using electron beam irradiation techniques or atmospheric pressure plasma [19,20]. This, as well as other modelling plasma applications [21], point to the requirement for precise and thorough electron scattering data for furfural [22].

Further, with rising of the energy consumption, worldwide difficulties related to collecting and storing energy sustainably are becoming increasingly important. Knowing and imitating nature may allow developments that could assist in addressing these issues. The principal method for conversion of the energy on Earth is oxygenic photosynthesis, in which H_2O and CO_2 are transformed into O_2 and sugars [23]. Hence, improving our knowledge of these photosynthetic pathways may spur advancements in photo catalysis and photovoltaics [24] as well as the development of hybrid photo-bio electrochemical technologies [25]. Within the cellular respiration and electron transport sequence of photosynthesis, quinones are crucial molecular component since they are capable of performing reversible reduction process. As a result, they are proving to be a viable option as a long-term, cost-effective material in energy-storage and harvesting systems, such as artificial photosynthetic platforms, dye-sensitized solar cells, phototransistors, rechargeable batteries, plasmonic light harvesting, and pseudo-capacitors. The development of bio-inspired energy conversion and harvesting devices can be facilitated by an understanding of the special properties of quinone and its derivatives [26]. In this context, para-benzoquinone (pBQ), the simplest quinone, has served as a prototype structure in a variety

of research seeking to understand the electrochemical and photo induced behavior of quinones in general [26].

Applications for fluoro- and perfluoro-organic compounds are numerous. Polyfluoroalkyl substances (PFSs) are been widely used in various industrial and commercial products. These (PFSs) can degrade to persistant perfluorocarboxylates (PFCAs) and perfluoroalkyl sulfonates (PFSAs). Perfluorinated carboxylic acids (PFCAs) are substances of significant environmental interest and concern over the past decade. PFCAs and their salts have been widely used as emulsifying agents in polymer synthesis and surface treatment agents in photolithography, paper coatings, waxes, and polishes [27]. They are also found to be widely distributed in the environent. They have also been discovered in human and animal tissues [28], ambientwater and wastewater plants [29].Due to their bioaccumulation and environmental persistence it is danger to humans and other animals [30].

4.2 Family Of Bio-Molecules In Aqueous Phase

In this section, elastic and inelastic effects of hydrated bio-molecules like Adenine, Guanine, Cytosine, Thymine and Uracil are widely studied.

4.2.1 Literature survey of present hydrated DNA targets

Table 4.1 shows the literature data for the present investigation.

Table 4.1 Literature survey of bio-molecules on the present study

Sr. No.	Quantity	Phase considered	Energy range (eV)	Theoretical Method	References
1	Q_{inel}	Molecules in water	20-10000	Dielectric response theory	Tan 2004 (Z. Tan et al., 2004)
2	Q_{ion}	Condensed phase	10-500		Tan 2018 (H. Q. Tan et al., 2018)

3	Q_{ion}		1-10000		Vera 2021 (de Vera et al., 2021)

4.2.2 Properties of present bio-molecules

Properties of the Present Compounds, which are used for computations, are tabulated in table 4.2.

Table 4.2 Molecular characteristics of present bio-molecules

Target	**Aqueous phase *IE* (eV)** [31,32]	E_{gap} **(eV)**
Adenine	5.00	5.25 [33]
Cytosine	5.50	5.35 [34]
Guanine	4.80	4.80 [35]
Thymine	5.40	5.20 [36]
Uracil	5.55	5.70 [34]

In figure 4.1, a schematic diagram of the present compounds has been shown.

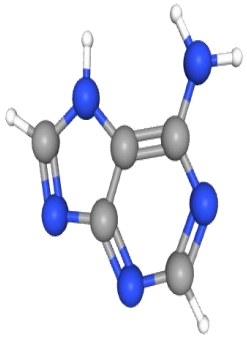

Adenine ($C_5H_5N_5$)

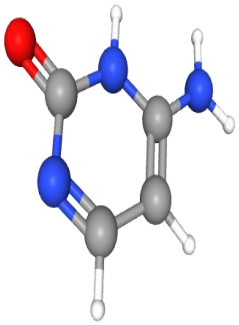

Cytosine ($C_4H_5N_3O$)

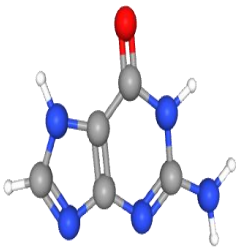

Guanine ($C_5H_5N_5O$)

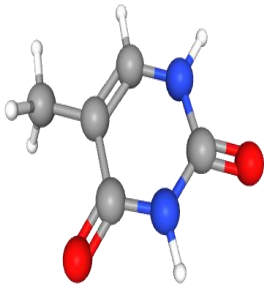

Thymine ($C_5H_6N_2O_2$)

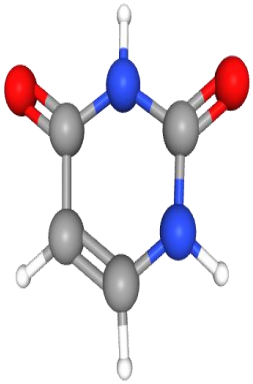

Uracil ($C_4H_4N_2O_2$)

Figure 4.1 Schematic representation of Present hydrated DNA molecules

(https://pubchem.ncbi.nlm.nih.gov)

4.2.3 Electron induced total cross sections for aqueous DNA molecules

In this section, we present the results on Q_{inel}, Q_{ion}, Q_{el} and Q_T for the aqueous DNA compounds, by employing SCOP, CSP-ic and 2p-SEM. We also report various correlations of peak ionization leading to prediction of dipole polarizability (α) and dielectric constant (ε) for all the present aqueous molecules.

(A) Inelastic contributions:

Through figures 4.2, 4.4, 4.6, 4.8 and 4.10, Q_{inel} and Q_{ion} are displayed for the investigated aqua-DNA constituents as a function of the electron energy along with the available results [13–15].

(B) Elastic contributions:

We have computed the elastic CSs (Q_{el}) and the total CSs (Q_T) for the electron energies from molecular IE to 5000 eV using the SCOP and 2p-SEM approach. Figures 4.3, 4.5, 4.7, 4.9 and 4.11 show the Q_{el} and Q_T plots against the incident electron energies for aqueous Adenine, Cytosine, Guanine, Thymine and Uracil, respectively. The results obtained from 2p-SEM and those from SCOP formalism are seen in good agreement with each other confirming the recently developed 2p-SEM method for larger and complex molecules. The Q_{el} results from both the methodologies (2p-SEM and SCOP) are observed to be in good accord with each other for all the present studied molecules, which validate the newly proposed 2p-SEM formalism even for the aqueous phase molecules.

4.2.4 Adenine

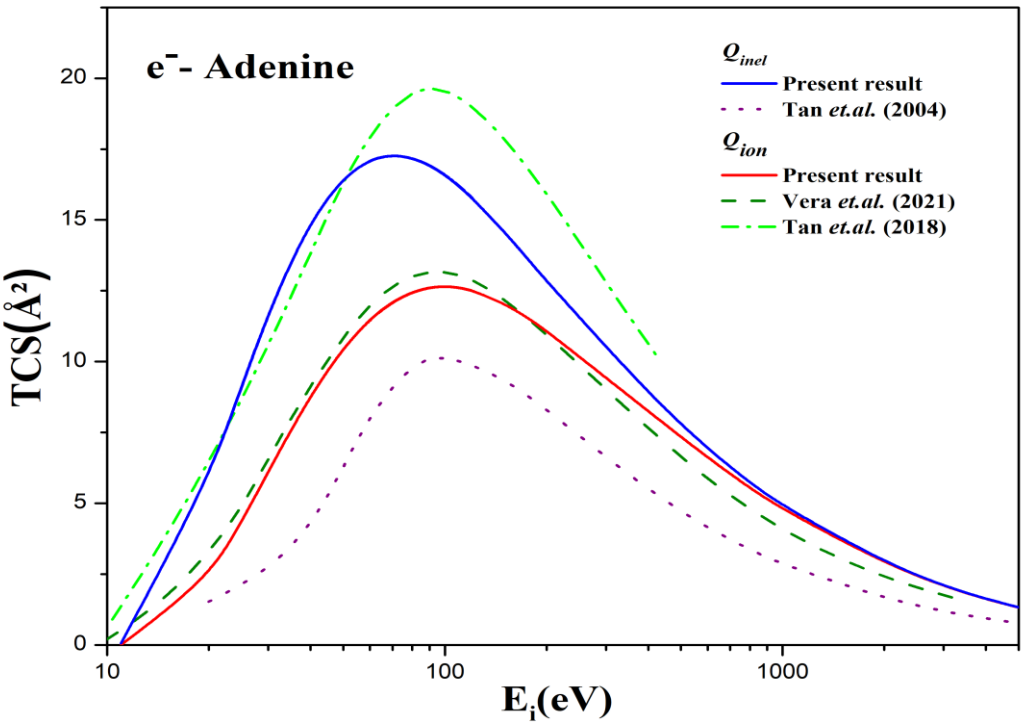

Figure 4.2 Inelastic interaction CSs for Adenine

Blue solid curve: Q_{inel}(Present); dotted curve: Tan et.al. Q_{inel} [13]**; Red solid curve: Q_{ion}(Present); dashed curve: Vera et.al. Q_{ion}** [14]**; dash Dot curve: Tan et.al. Q_{ion}** [15]

In figure 4.2, inelastic processes for adenine are shown. Top curves show total inelastic cross sections, Q_{inel}. Tan *et.al.* [13] have reported the Q_{inel} data for the case of DNA in water using dielectric response theory and Penn's approximation.However, their Q_{inel} underestimate present Q_{inel} and have lower values than even all the reported Q_{ion}. In figure 4.3, 2p-SEM and SCOP techniques used and with the help of it Q_{el} and Q_T has reported.

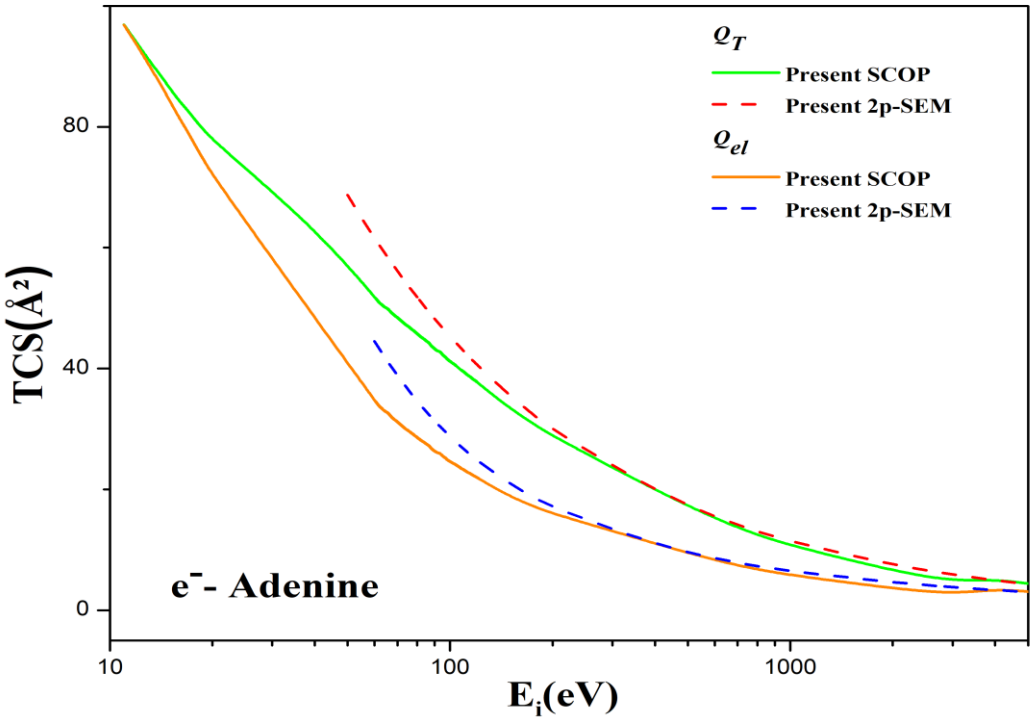

Figure 4.3 Elastic and total interaction CSs for Adenine

Green solid curve: SCOP Q_T(Present); red dashed curve: 2p-SEM Q_T(Present); Orange solid curve: SCOP Q_{el}(Present); blue dashed curve: 2p-SEM Q_{el}(Present)

Table 4.3 lists the calculated TCS values for Adenine.

Table 4.3 Total cross-sections (Å^2) for Adenine molecule

E_i (eV)	Q_{ion}	Q_{el}	Q_T
11	0.004	96.823	96.883
20	2.354	72.017	77.853
40	8.761	48.424	63.274
60	11.463	34.785	51.864
70	12.081	31.174	48.432
80	12.429	28.593	45.756

90	12.6	26.344	43.261
100	12.646	24.6	41.18
200	11.089	15.984	28.827
400	8.247	11.039	19.906
600	6.609	8.24	15.162
800	5.54	6.742	12.469
1000	4.786	5.809	10.718
2000	2.886	3.61	6.527
3000	2.073	2.692	4.778
4000	1.618	3.483	5.108
5000	1.325	3.073	4.402

4.2.5 Guanine

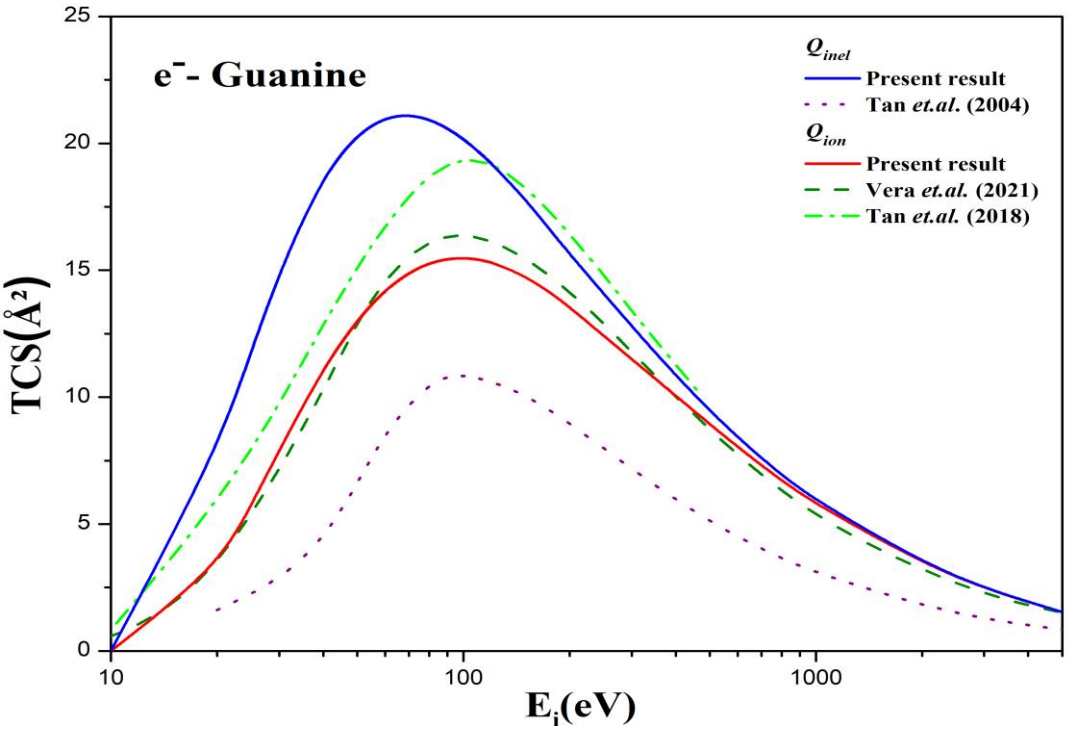

Figure 4.4 Inelastic interaction CSs for Guanine

Blue solid curve: Q_{inel}(Present); dotted curve: Tan et.al. Q_{inel} [13]**; Red solid curve: Q_{ion}(Present); dashed curve: Vera et.al. Q_{ion}** [14]**; dash Dot curve: Tan et.al. Q_{ion}** [15]

Figure 4.4 depicts inelastic effects for guanine. The top curves represent complete inelastic cross sections, denoted by Q_{inel}. Tan et.al. [13] used dielectric response theory and Penn's approximation to publish the Q_{inel} data for the case of DNA in water. In figure 4.5, 2p-SEM and SCOP methods were applied, and Q_{el} and Q_T reported using them.

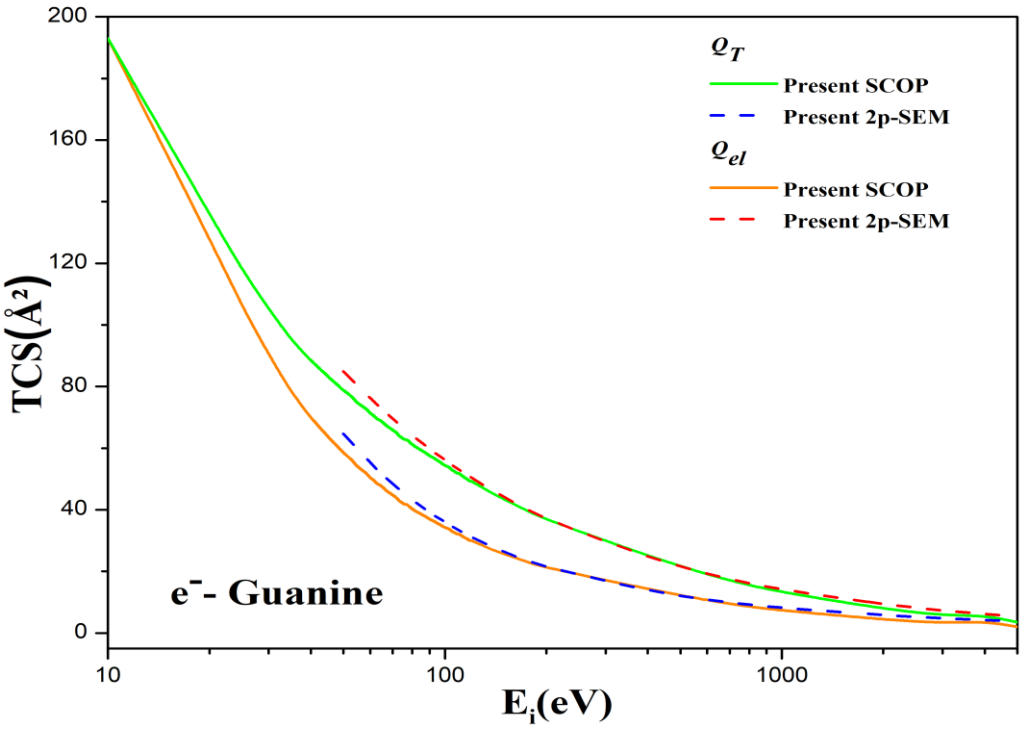

Figure 4.5 Elastic and total interaction CSs for Guanine

Green solid curve: SCOP Q_T(Present); red dashed curve: 2p-SEM Q_T(Present); Orange solid curve: SCOP Q_{el}(Present); blue dashed curve: 2p-SEM Q_{el}(Present)

Table 4.4 lists the calculated TCS values for Guanine.

Table 4.4 Total cross-sections (Å²) for Guanine molecule

E_i (eV)	Q_{ion}	Q_{el}	Q_T
10	0	192.948	192.953
20	3.269	128.232	136.078
30	7.896	90.453	105.292
40	11.038	69.997	88.507
50	12.99	58.51	78.758

60	14.174	50.404	71.351
70	14.87	44.76	65.843
80	15.254	40.281	61.196
90	15.431	36.984	57.564
100	15.47	34.257	54.412
200	13.555	21.219	36.855
400	10.044	14.296	25.072
600	8.024	10.587	18.979
800	6.705	8.558	15.482
1000	5.779	7.344	13.267
2000	3.46	4.378	7.874
3000	2.477	3.166	5.658
4000	1.932	3.834	5.774
5000	1.53	2.004	3.538

4.2.6 Cytosine

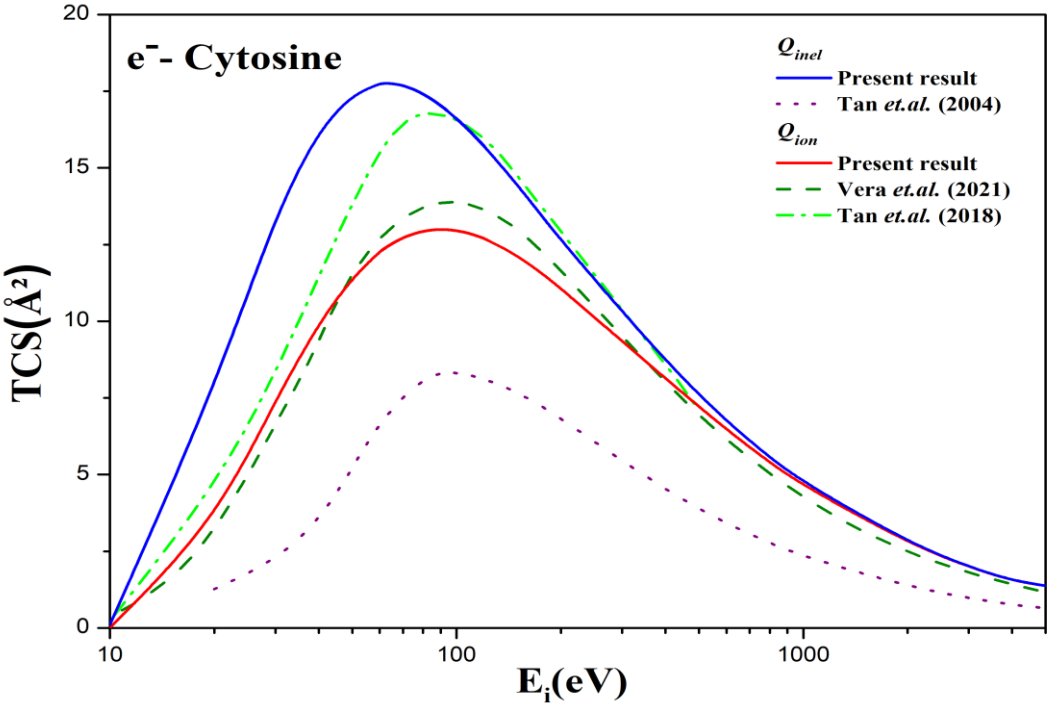

Figure 4.6 Inelastic interaction CSs for Cytosine

Blue solid curve: Q_{inel}(Present); dotted curve: Tan et.al. Q_{inel} [13]**; Red solid curve: Q_{ion}(Present); dashed curve: Vera et.al. Q_{ion}** [14]**; dash Dot curve: Tan et.al. Q_{ion}** [15]

The solid curves shows Q_{inel} and Q_{ion} respectively**.** The available comparisons are shown in figure 4.6. They took an equivalent unit of DNA molecule in water environment with 50% Guanine-Cytosine and 50% Adenine-Thymine and then separated into 5 constituents of DNA. In figure 4.7, Q_{el} and Q_T using SCOP and 2p-SEM methods are shown. They match well over the entire range of energy.

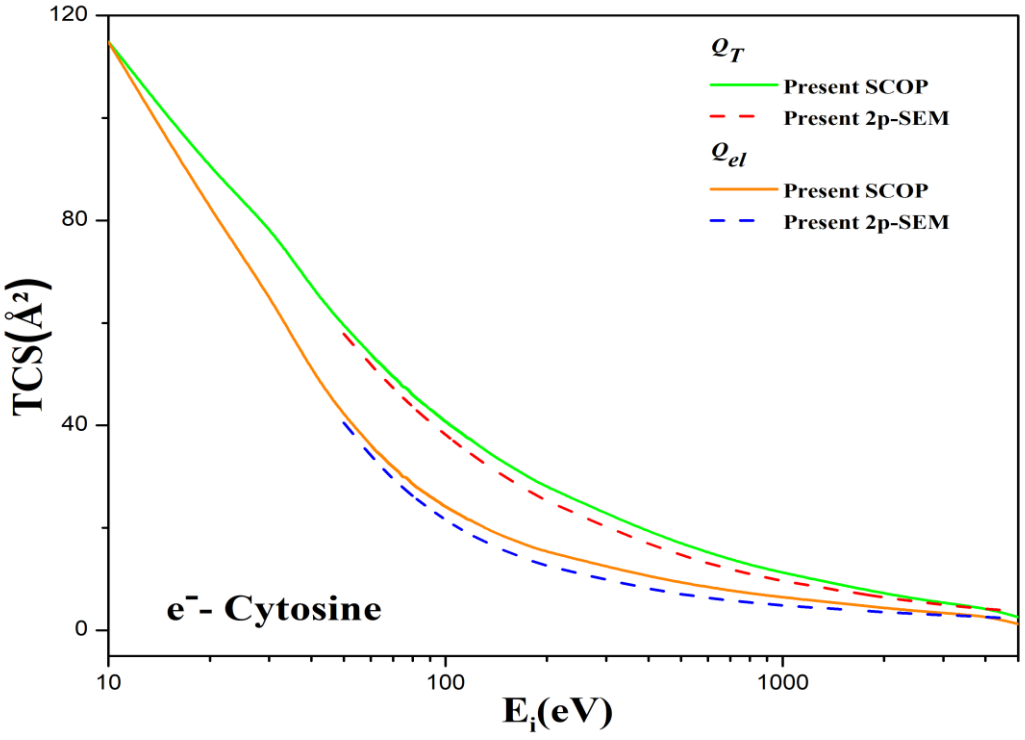

Figure 4.7 Elastic and total interaction CSs for Cytosine

Green solid curve: SCOP Q_T(Present); Red dashed curve: 2p-SEM Q_T(Present); Orange solid curve: SCOP Q_{el}(Present); Blue dashed curve: 2p-SEM Q_{el}(Present)

Table 4.5 lists the calculated TCS values for Cytosine.

Table 4.5 Total cross-sections (Å²) for Cytosine molecule

E_i (eV)	Q_{ion}	Q_{el}	Q_T
10	0.008	114.813	114.917
20	3.422	82.112	89.876
30	7.418	65.542	79.035
40	9.939	50.7	66.938
50	11.416	42.006	59.397
60	12.258	36.262	54.002

70	12.714	31.814	49.493
80	12.927	28.52	45.926
90	12.988	26.111	43.139
100	12.948	24.149	40.748
200	11.07	15.315	27.955
400	8.13	10.448	19.121
600	6.471	8.419	15.161
800	5.395	7.226	12.781
1000	4.643	6.458	11.206
2000	2.769	4.33	7.125
3000	1.979	3.351	5.341
4000	1.546	2.797	4.348
5000	1.372	1.225	2.602

4.2.7 Thymine

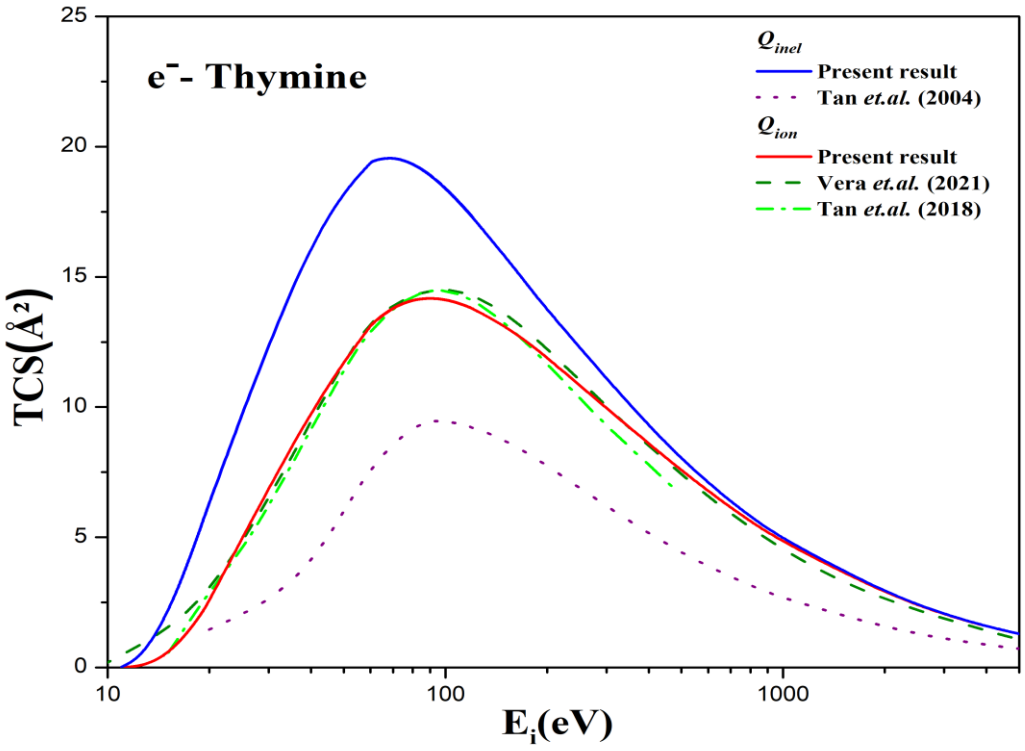

Figure 4.8 Inelastic interaction CSs for Thymine

Blue solid curve: Q_{inel}(Present); dotted curve: Tan et.al. Q_{inel} [13]**; Red solid curve: Q_{ion}(Present); dashed curve: Vera et.al. Q_{ion}** [14]**; dash Dot curve: Tan et.al. Q_{ion}** [15]

Q_{ion} and Q_{inel} are shown in figure 4.8. The current study's Q_{ion} shows good agreement with existing comparisons over the whole energy range. Tan *et.al.* [15] and Vera *et.al.* [14] have reported the Q_{ion} data for condensed DNA bases using the methodologies which underlines the dielectric response theory. The present results of Q_{ion} are observed to be in good accord with those of Vera *et.al.* (de Vera et al., 2021). Figure 4.9 depicts Q_{el} and Q_T utilising SCOP and 2p-SEM techniques. They match nicely over the full energy spectrum.

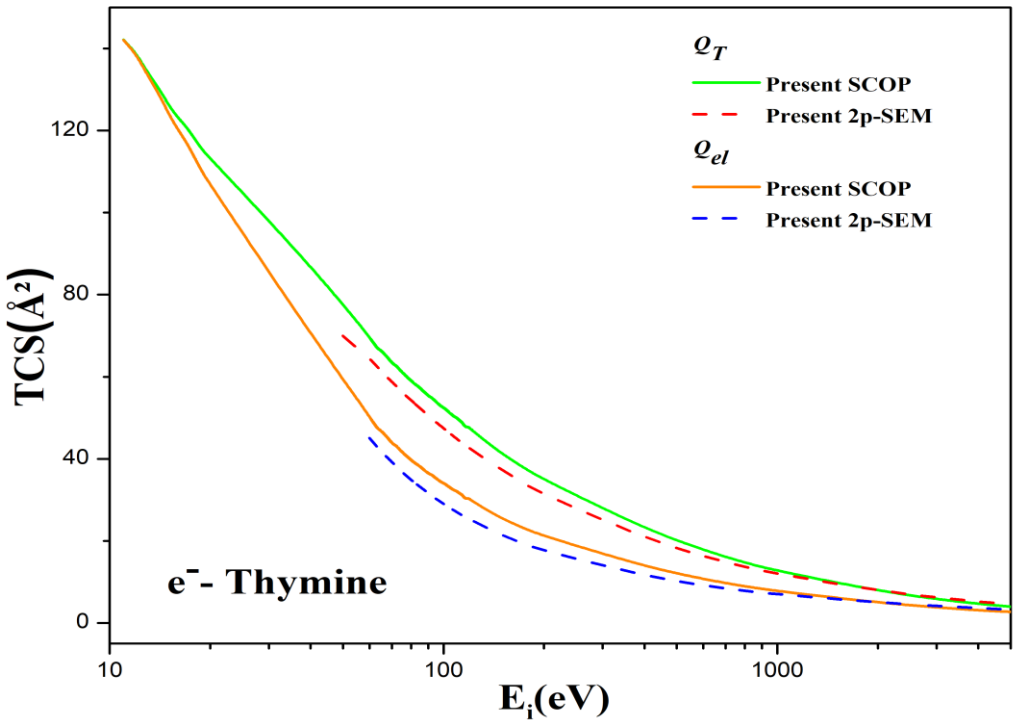

Figure 4.9 Elastic and total interaction CSs for Thymine

Green solid curve: SCOP Q_T(Present); Red dashed curve: 2p-SEM Q_T(Present); Orange solid curve: SCOP Q_{el}(Present); Blue dashed curve: 2p-SEM Q_{el}(Present)

Table 4.6 lists the calculated TCS values for Thymine.

Table 4.6 Total cross-sections (Å²) for Thymine molecule

E_i (eV)	Q_{ion}	Q_{el}	Q_T
11	1.00E-03	142.101	142.119
20	2.547	106.867	113.226
40	10.009	70.344	87.167
60	13.126	50.412	69.811
70	13.788	43.969	63.518

80	14.094	39.719	59.045
90	14.174	36.536	55.441
100	14.115	34.052	52.444
200	11.908	21.225	34.963
400	8.577	13.728	22.928
600	6.758	10.708	17.773
800	5.604	8.884	14.668
1000	4.805	7.741	12.663
2000	2.843	4.951	7.822
3000	2.032	3.778	5.821
4000	1.574	3.098	4.678
5000	1.291	2.689	3.983

4.2.8 Uracil

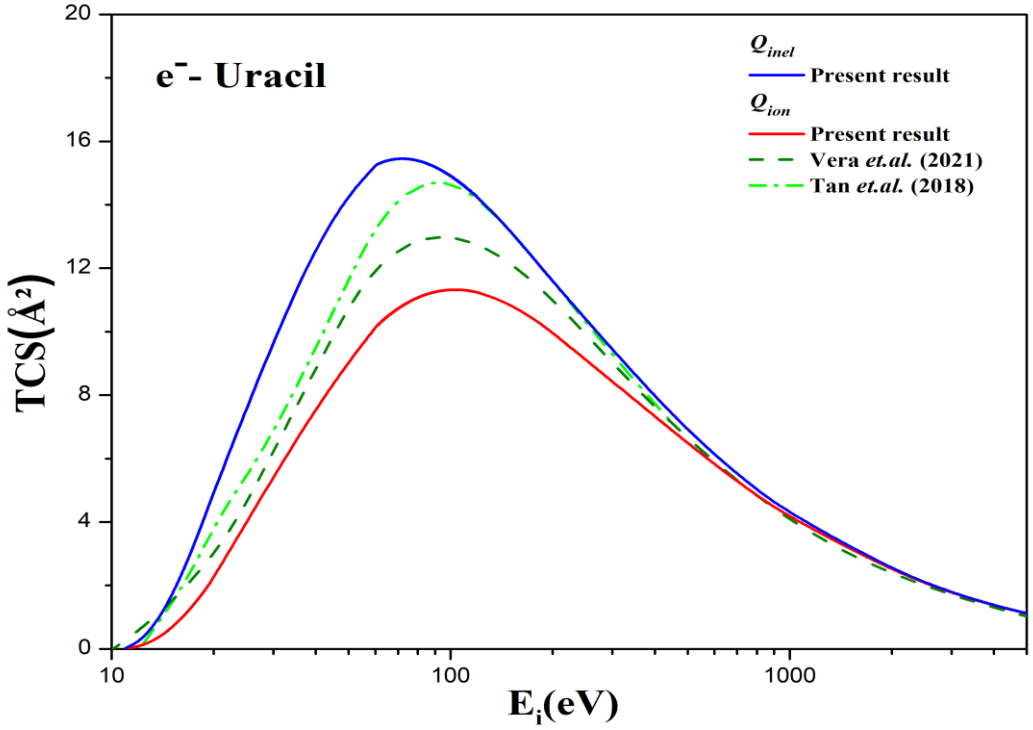

Figure 4.10 Inelastic interaction CSs for Uracil

Blue solid curve: Q_{inel}(Present); Red solid curve: Q_{ion}(Present); dashed curve: Vera et.al. Q_{ion} [14]**; dash Dot curve: Tan et.al. Q_{ion}** [15]

In figure 4.10, present Q_{ion} and Q_{inel} of uracil have shown. As can be seen, the data of Tan *et.al.* [15] overestimate both, present data and those of Vera *et.al.* [14]. The minute deviation at the peak value of Q_{ion} may be because of the consideration of the different phases for the molecules. Q_{el} and Q_T are shown in Figure 4.11 using SCOP and 2p-SEM methods. They complement each other well over the whole energy spectrum.

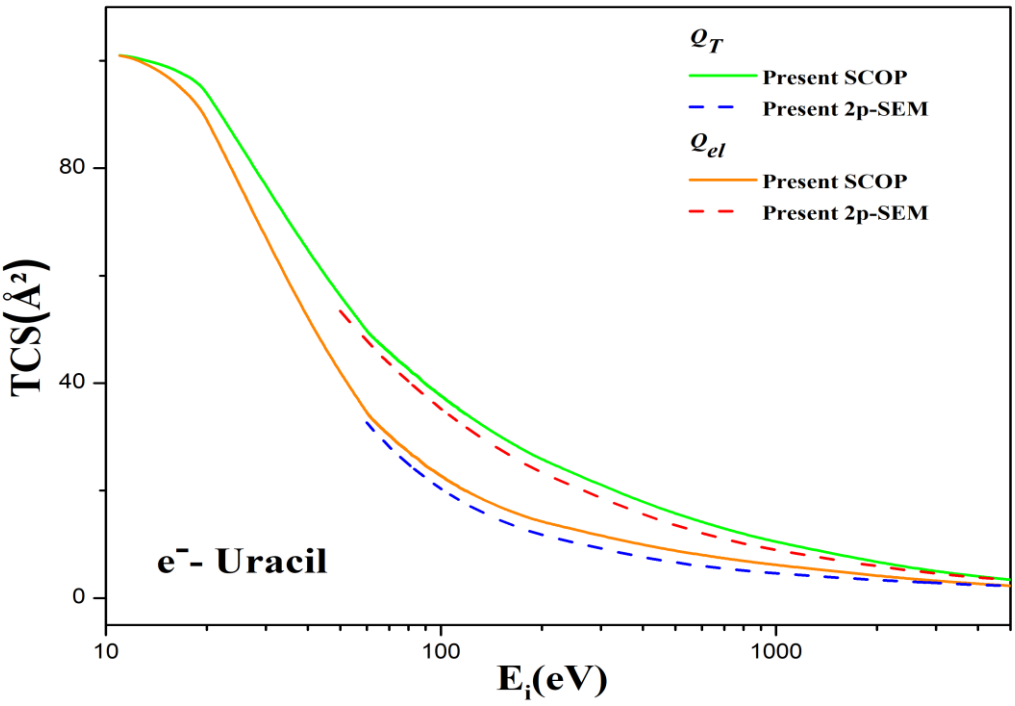

Figure 4.11 Elastic and total interaction CSs for Uracil

Green solid curve: SCOP Q_T(Present); Red dashed curve: 2p-SEM Q_T(Present); Orange solid curve: SCOP Q_{el}(Present); Blue dashed curve: 2p-SEM Q_{el}(Present)

Table 4.7 lists the calculated TCS values for Uracil.

Table 4.7 Total cross-sections (Å²) for Uracil molecule

E_i (eV)	Q_{ion}	Q_{el}	Q_T
11	0.007	100.964	100.986
20	2.24	89.437	94.386
40	7.689	50.974	64.102
60	10.143	34.534	49.785
70	10.731	30.299	45.747

80	11.075	27.231	42.621
90	11.255	24.618	39.807
100	11.32	22.712	37.618
200	9.974	14.147	25.728
400	7.327	9.783	17.689
600	5.811	8.004	14.114
800	4.832	6.896	11.911
1000	4.149	6.143	10.415
2000	2.463	4.126	6.623
3000	1.761	3.199	4.976
4000	1.369	2.656	4.034
5000	1.119	2.306	3.431

4.3 Furfural And Parabenzoquinone Compounds

In this section, inelastic and elastics effects for furfural and parabenzoquinone from energy range IP to 5keV are discussed and compare it with available comparisons.

4.3.1 Literature survey and properties of furfural and PBQ targets

Table 4.8 shows the previous studies of furfural and parabenzoquinone molecules.

Table 4.8 Literature survey of furfural and PBQ targets

Compound	CSs	Methods	E_i (eV)	References
$C_5H_4O_2$	Q_{ion}	Binary-Encounter-Bethe (BEB) [Th.]	1-1000	Jones *et al* (2016) [22]
	Q_{inel}, Q_{el}, Q_T	IAM-SCAR+I [Th.]		
	ΣQ_{exc}	Energy loss spectra [Ex.]	20,30,40,50,250	
	ΣQ_{exc}	Discrete inelastic [Th.]	1-1000	
	Q_T	Double electrostatic analyzer gas cell electron transmission cell [Ex.]	10-1000	Traore Dubuis *et al* (2017) [37]
	Q_T	IAM-SCAR+I [Th.]	500-10000	
	Q_T	Electron Transmission Experiment [Ex.]	7, 10, 20	Lozano *et al* (2017) [38]
$C_6H_4O_2$	Q_T	Transmission-beam attenuation measurements [Ex. ±5%]	1-200	Lozano *et al* (2018) [39]
	Q_{inel}, Q_{ion}, Q_{el}, Q_T, ΣQ_{exc}	IAM-SCAR+I [Th.]		
	Q_{el},	SMCPP [Th.]	1-50	
	ΣQ_{exc}	Energy loss spectra [Ex.]	20,30,40	Jones *et al* (2018) [40]
	Q_{inel}, Q_{el}, Q_T, ΣQ_{exc}	IAM-SCAR+I [Th.]	10-1000	
	Q_{ion}	BEB [Th.]	10-1000	
	Q_{inel}, Q_{el}, Q_T, Q_{ex}	SMCPP [Th.]	16-50	

4.3.2 Target properties of furfural and PBQ compounds

The target properties for furfural and PBQ compounds are shown in table 4.9.

Table 4.9 Targets properties of Furfural and PBQ Compounds

Target	IE (eV)	Polarizability (α)	
		($A°^3$)	**(a_0^3)**
Furfural ($C_5H_4O_2$)	9.21	10.0	67.55
Parabenzoquinone ($C_6H_4O_2$)	10.01	10.8	72.95

Figure 4.12 shows a schematic diagram of the furfural and parabenzoquinone.

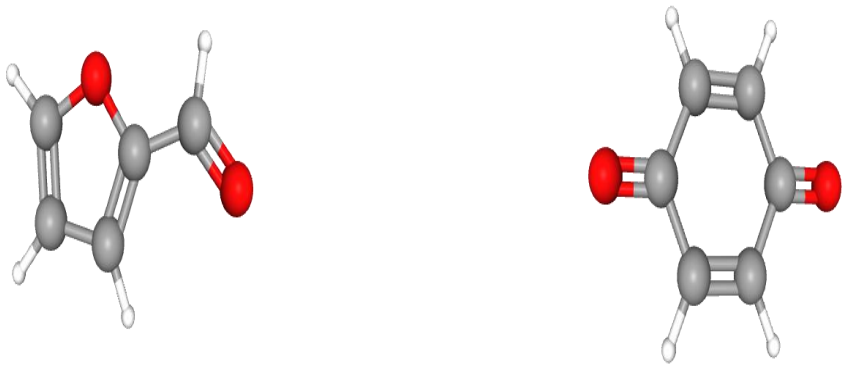

Furfural **Parabenzoquinone**

Figure 4.12 Schematic diagram of the furfural and parabenzoquinone

4.3.3 Furfural

In the present work we have calculated various cross sections (Q_{inel}, Q_T, Q_{el}, Q_{ion}, and ΣQ_{exc}) for electron interactions with furfural ($C_5H_4O_2$) for the impact energy starting from IE to 5000 eV. To compute Q_{inel}, Q_{el} and Q_T, SCOP formalism has been employed and CSP-ic approach

has been used to bifurcate the Q_{inel} into Q_{ion} & ΣQ_{exc}. To facilitate our discussion present theoretical results are plotted in figures 4.13 and 4.14 along with the available comparisons.

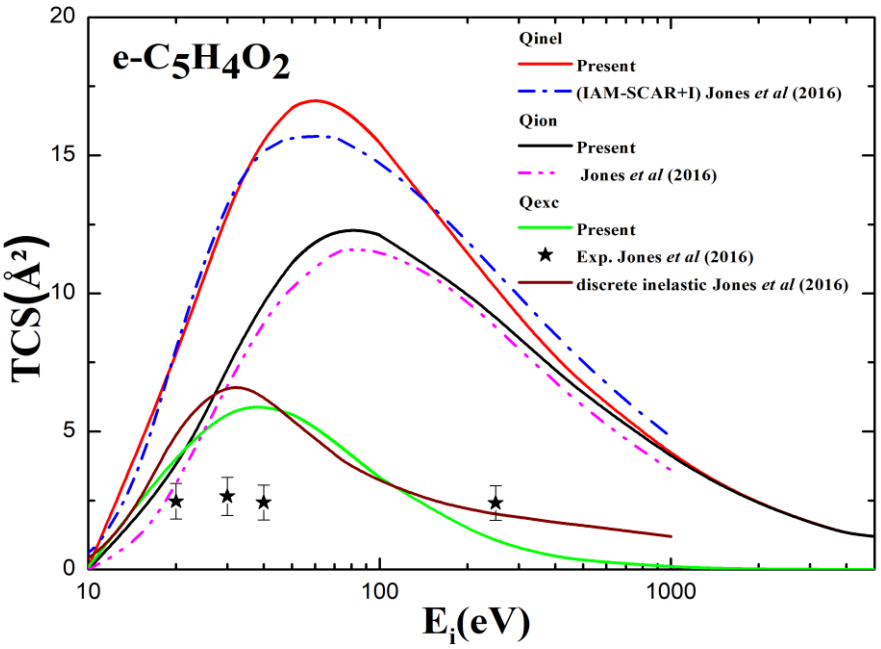

Figure 4.13 Present Q_{inel}, Q_{ion}, and ΣQ_{exc} cross section for e-$C_5H_4O_2$

Q_{inel}: Dash - Present, Dash dot - Jones et at [22] **(IAM-SCAR+I), Q_{ion}: Solid - Present, Dash dot dot - Jones et at** (Jones, da Costa, et al.,2016)**, ΣQ_{exc}: Short dash-Present, filled star- Jones et at** [22] **(exp.), Short dot- Jones et al discrete inelastic**

Present inelastic, ionization, and excitation cross sections for e-furfural are plotted in Figure 4.13. The topmost curve shows Q_{inel}, which is compared with the only available data of Jones *et.al.* [22]. They used IAM-SCAR+I method for energies from 1 to 1000 eV. Starting from the threshold to peak of the impact energy, present Q_{inel} shows excellent accord with that of Jones *et.al.* [22]. However, at the peak region present Q_{inel} overestimates the IAM-SCAR+I curve. (Reason- Jones et.al. Q_{inel} involves the contribution of rotational excitations also) The present Q_{ion} is shown through the middle solid line in Figure 4.13. Only Jones *et.al.* [22] has reported the Q_{ion} results using BEB theory and present data are seen to be in good accord with them within the mentioned 15% uncertainty of BEB. The lowest curve represents the calculated

$\sum Q_{exc}$. It is compared with both theoretical and experimental excitation cross sections of Jones *et.al.* [22]. Their calculated data overestimates the present $\sum Q_{exc}$. The experimental electronic excitation cross-sections for the bands I-VI separately and their $\sum Q_{exc}$ (band I+II+III+IV+V+VI)), both are reported by Jones *et.al.* [22] for the energy range 20-250 eV with the mentioned uncertainty 18% to 69%. This summed Q_{exc} is compared and seen to be of lower values than present $\sum Q_{exc}$(calculated for all the allowed electronic excitations), as expected.

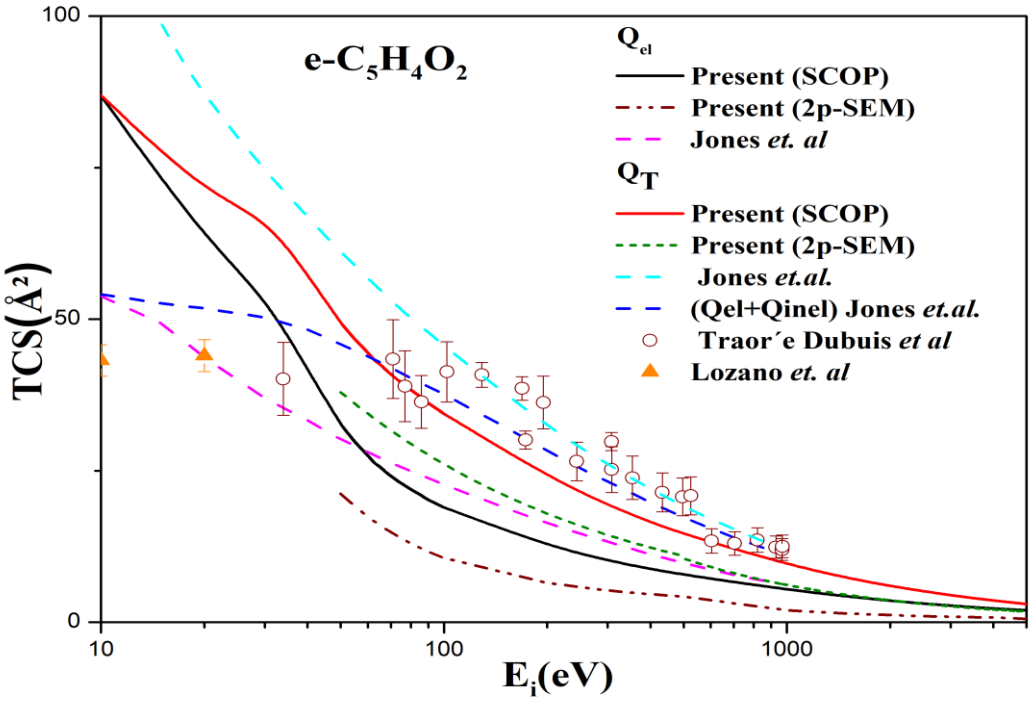

Figure 4.14 Present Q_{el} and Q_T cross section for e-$C_5H_4O_2$

Q_{el}: Dot -Present (SCOP), Dash dot dot -Present (2p-SEM), Dash - Jones et al [22], **Q_T: Solid - Present (SCOP), Short dash- Present (2p-SEM), Dash - Jones et al** [22] **(complete), short dash dot- Jones et al** [22] **(Q_{el}+Q_{inel}), solid circle- Traor´e Dubuis et al** [37], **Solid triangle- Lozano et al** [38], **Dash - Traor´e Dubuis et al** [37]**(SEM)**

In figure 4.14 present Q_{el} and Q_T are illustrated for the electron collision with Furfural molecule. The only data of Jones *et.al.* [22] for Q_{el} has been compared with the present one. At low energies a high disagreement between both of them can be observed, which is due to the fact that the present Q_{el} has been calculated in the presence of inelastic channels while Jones et.al. has computed the pure Q_{el}. Authors reported uncertainty ICS by up to 43% at 1000 eV due to interference term added in the calculation of elastic ICS. The Q_T calculated using

present SCOP method is also plotted in figure 4.4 with the existing data of Jones *et.al.* [22], Lozano *et.al.* [38] and Traoré Dubuis *et.al.* [37]. The discrepancies between the present data and all the available data can be observed from the figure 4.14. However, the present results of Q_T show the same trend as that of Jones et.al. [22]. While present calculation does not involve the non-spherical effects, Jones et.al. [22] have considered the involvement of rotational excitations into Q_T. This may be the reason for the discrepancy between the present data and results of Jones et.al. [22]. The experimental Q_T data of Traoré Dubuis *et.al.* [37] also seen in reasonable agreement with the present ones within the mentioned uncertainty of 4% - 22% above 50 eV [37]. Traoré Dubuis *et.al.* [37] have also calculated the Q_T for energy above 500 eV, using a two-parameter semi-empirical model (SEM) proposed by Garcia and Manero [41] for molecules having up to 22 electrons. This SEM results tend to merge with the present Q_T at high energies.

TCS values for furfural are listed in table 4.10.

Table 4.10 Total cross-sections (Å^2) for Furfural molecule

E_i (eV)	Q_{ion}	Q_{el}	Q_T
10	0.007	86.836	86.923
20	3.399	63.375	70.951
30	7.323	53.77	66.878
40	9.731	41.655	57.344
50	11.098	32.697	49.416
60	11.841	27.513	44.487
70	12.183	24.124	40.928
80	12.281	21.946	38.367
90	12.241	20.2	36.153
100	12.122	18.945	34.404

200	10.046	12.662	24.111
300	8.398	10.189	19.351
400	7.234	8.816	16.53
500	6.37	7.847	14.545
1000	4.061	5.401	9.554
1500	3.015	4.257	7.314
2000	2.403	3.559	5.984
2500	2.006	3.094	5.113
3000	1.715	2.752	4.476
3500	1.494	2.489	3.99
4000	1.327	2.283	3.614
4500	1.25	2.123	3.294
5000	1.2	1.983	3.014

4.3.4 Para-Benzoquinone

In this section, we examined various cross-sectional quantities for electron scattering with Para-Benzoquinone ($C_6H_4O_2$) such as total ionization, total inelastic and discrete excitation in figure 4.15 and total elastic cross section in figure 4.16 and upper bound total cross section in figure 4.17 with available comparisons.

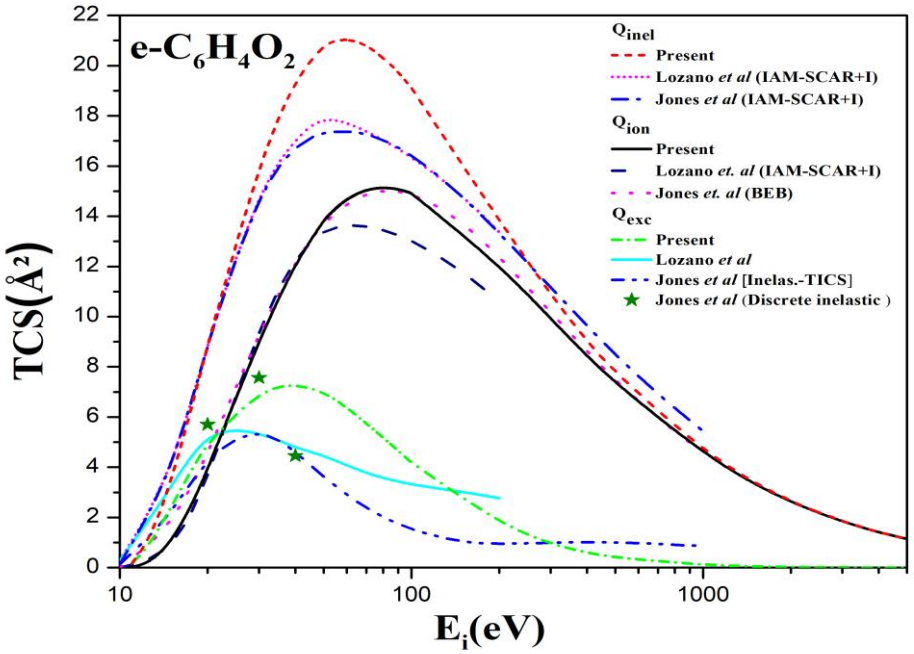

Figure 4.15 Present Q_{inel} , Q_{ion} , and ΣQ_{exc} cross section for e-$C_6H_4O_2$

Q_{inel}: short dash -Present, short dot - Lozano et al [39] **(IAM-SCAR+I), dash dot - Jones et al** [40] **(IAM-SCAR+I), Q_{ion}; solid -Present, dash -Lozano et al** [39] **(IAM-SCAR+I), dot - Jones et at** [40] **(BEB), ΣQ_{exc}; short dash dot -present, dash dot dot - Jones et al** [40] **(Inelas.-TICS), solid star- Jones et al** [40] **(Discrete inelastic)**

Figure 4.15 displays the Q_{inel} for e^--$C_6H_4O_2$ collision with available theoretical comparisons of Lozano *et.al.* [39] and Jones *et.al.* [40]. Both the authors [39] employed IAM-SCAR+I approach and produced Q_{inel} results, which are of quite lower values than the present Q_{inel} at the peak region. Except the peak region, present results overlap with the existing ones. Also in figure 4.15, we represent ΣQ_{exc} computed through present methodology along with the available comparisons. The theoretical excitation cross sections calculated using IAM-SCAR+I method [39], [40] are observed to be in good agreement with the present results below 25 eV, afterwards they underestimate the present ΣQ_{exc}. (Reason) Jones *et.al.* [40] has also measured the electronic excitation cross-sections for each bands 0-V from 20-40 eV energies. Their reported sum values have been compared here with the present ΣQ_{exc} and good agreement can be observed for 20 and 30 eV. Jones *et.al.* [40] has also reported the computed ΣQ_{exc} values

using Schwinger multichannel method with pseudopotential (SMCPP) calculations and the produced results largely deviate in comparison to other existing ones.

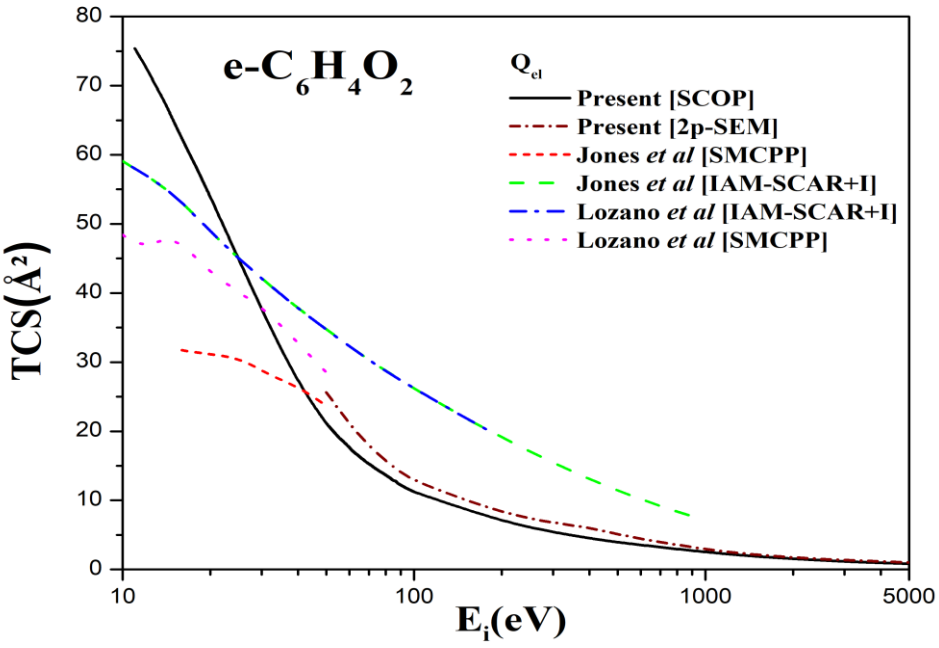

Figure 4.16 Q_{el} for e-$C_6H_4O_2$

Q_{el}: Solid - Present (SCOP), short dash- Present (2p-SEM), Dot- Lozano et al [39] **(SMCPP), dash dot -Lozano et al** [39] **(IAM-SCAR+I), dash- Jones et at** [40] **(IAM-SCAR+I), short dash- Jones et at** [40] **(SMCPP)**

In figure 4.16, present Q_{el} for e-$C_6H_4O_2$ collision along with the available Q_{el}, computed using IAM-SCAR+I and SMCPP approach has been plotted. At threshold to 30 eV our data are overestimated with both the IAM-SCAR+I and SMCPP methods. At higher incident energy our data of Q_{el} follows $ln(E)/(E)$ nature as might be expected as shown in figure 4.17.

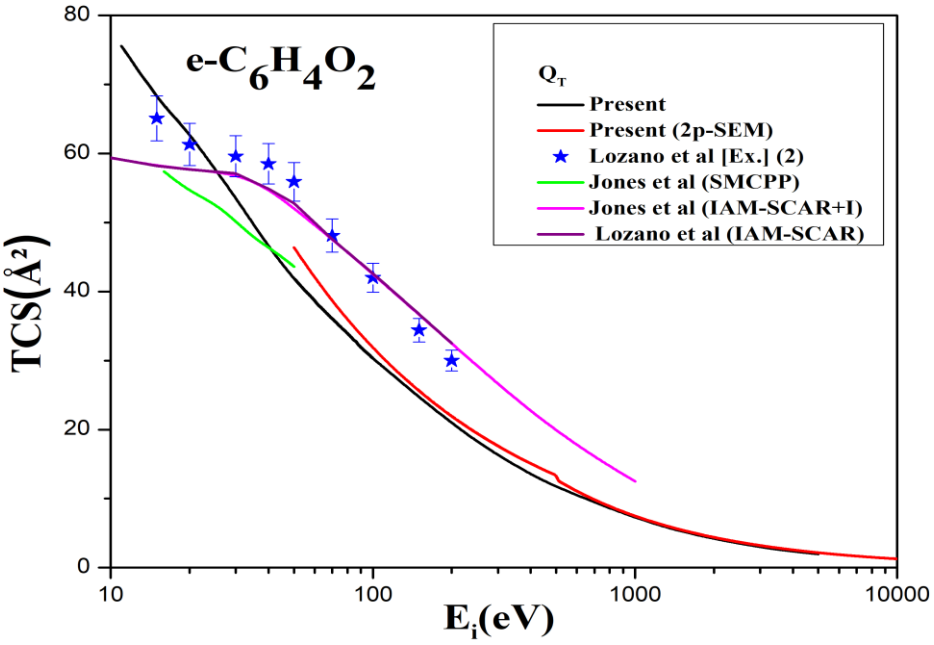

Figure 4.17 Q_T for e-$C_6H_4O_2$

Q_T: solid- Present, dash- Present (2p-SEM), solid star- Lozano *et al* [39] (Exp.), dot - Jones *et al* [40] (SMCPP), dash dot - Jones *et al* [40] (IAM-SCAR+I), short dash - Lozano *et al* [39] (IAM-SCAR+I)

Table 4.11 shows the computed TCS values for PBQ.

Table 4.11 Total cross-sections (Å²) for PBQ molecule

E_i (eV)	Q_{ion}	Q_{el}	Q_T
11	0.016	75.384	75.568
20	3.94	53.917	62.791
30	9.084	37.483	53.657
40	12.16	26.906	46.422

50	13.822	21.12	41.898
60	14.662	17.653	38.677
70	15.032	15.279	36.057
80	15.132	13.644	33.946
90	15.066	12.203	31.921
100	14.914	11.209	30.317
200	12.074	6.919	20.745
300	9.92	5.402	16.262
400	8.434	4.525	13.545
500	7.356	3.912	11.662
1000	4.548	2.49	7.146
1500	3.318	1.875	5.239
2000	2.624	1.545	4.193
2500	2.174	1.322	3.512
3000	1.85	1.162	3.022
3500	1.604	1.043	2.653
4000	1.412	0.956	2.374
4500	1.272	0.885	2.161
5000	1.142	0.837	1.983

The present total cross sections (Q_T) are the summation of Q_{el} and Q_{inel}. In figure 4.17, present Q_T data has been plotted for the energy range from IE to 10,000 eV. As mentioned earlier, the

computations for Q_T have been done using the SCOP formalism for the energies up to 5000 eV. To extend our data until 10,000 eV we have used the 2p-SEM approach discussed in the theory section. The theoretical results as well as experimental ones [39] are compared with the present Q_T data. From the figure 4.17, it can be observed that the present SCOP results for Q_T at lower energies find good agreement with the experimental results of Lozano *et.al.* [39] within the experimental uncertainty limit of ±5%.

4.4 Pentafluoropropionic Acid

In this section, inelastic and elastics effects for pentafluoropropionic acid (PFPA) ($C_3F_5HO_2$) from energy range IP to 5keV are discussed.

4.4.1 Molecular properties

In table 4.12, molecular properties of $C_3F_5HO_2$ are listed.

Table 4.12 Molecular properties of PFPA compound

Target	n_e	Ionization Potential (eV)	Polarizability ($10^{-24}cm^{-3}$)		
			Present	Estimated	Found at www.chemspider.com
$C_3F_5HO_2$	80	11.94	-	8.71	7.2 (deviation 20.97%)

In figure 4.18, schematics of PFPA is shown below.

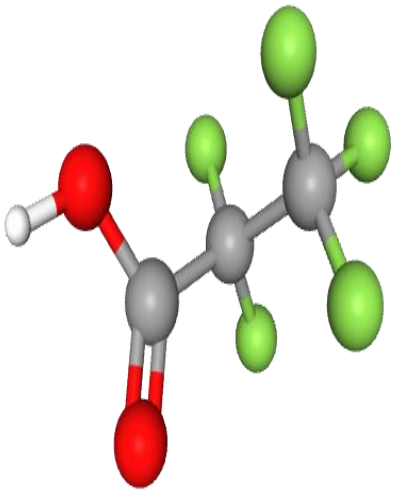

$C_3F_5HO_2$

Figure 4.18 Diagrammatic representations of $C_3F_5HO_2$ molecule

(https://pubchem.ncbi.nlm.nih.gov)

4.4.2 Inelastic and elastic effects on PFPA

In this section, various electron impact processes is described. There is no comparison data available for this compound.

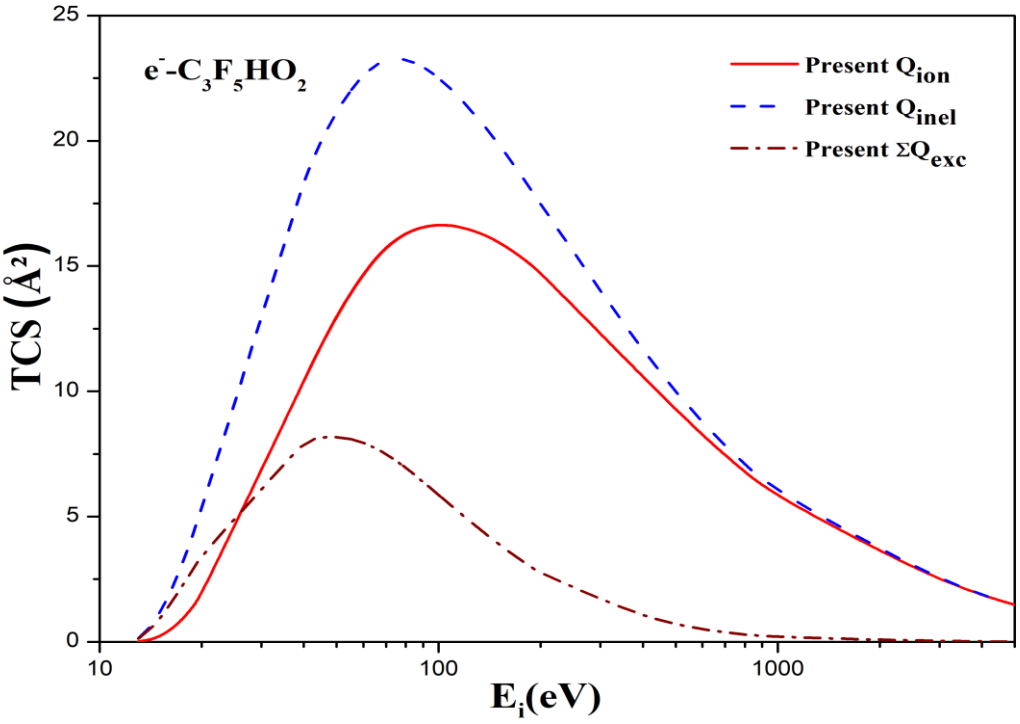

Figure 4.19 Inelastic processes for $C_3F_5HO_2$

Line: Present Q_{ion}, Dash: Present Q_{inel}, Dash dot: Present $\sum Q_{exc}$

As shown in figure 4.19, we provided the Q_{inel}, Q_{ion}, and ΣQ_{exc}. In below figure 4.20 shows the present Q_T and Q_{el} data for $C_3F_5HO_2$. We are unable to compare our results with any experimental and theoretical data as there are no previous results vailable. The cross sections for $C_3F_5HO_2$, we have employed the SCOP formalism to calculate elastic as well as inelastic cross sections and used CSP-ic method for ionization cross sections.

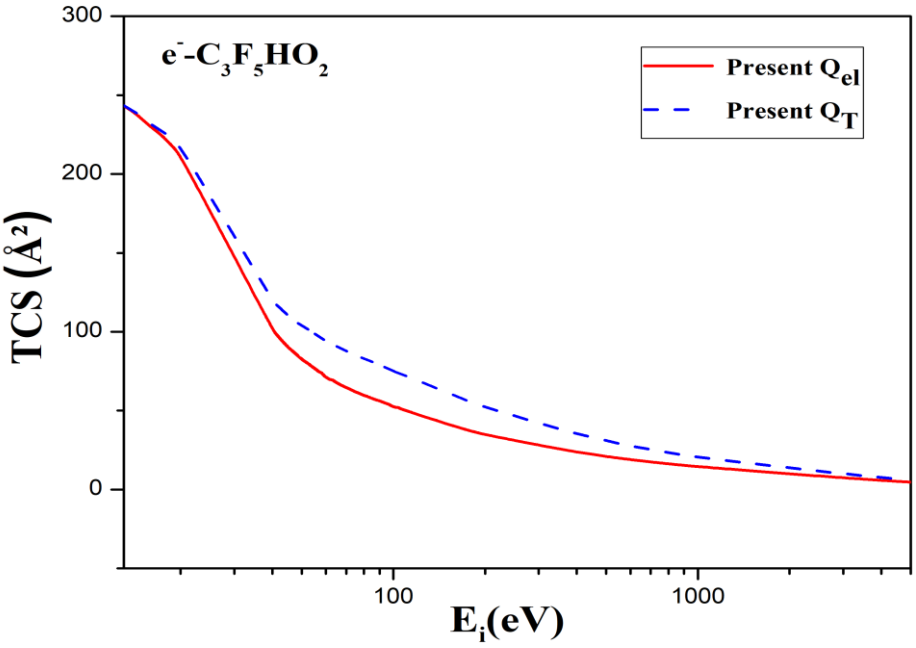

Figure 4.20 Elastic process and total cross section

Line: Present Q_{el}, Dash: Present Q_T

4.5 Trends Of Total Cross Section

In this section, we discussed various correlation among polarizability, dielectric constant and Q_{ion} and Q_T.

4.5.1 Various correlations: Prediction of polarizability (α) and dielectric constant (ε)

We have used the calculated total ionization cross sections to compute useful parameters, polarizability (α) and dielectric constant (ε) for aqua-DNA molecules, which are not found in literature.

4.5.2 Polarizability (α)

According to Harland's proposed qualitative dependency nature of the maximum ionization CSs, ($Q_{ion(m)}$) with its polarizability (α) [42],

$$Q_{ion(\mathrm{m})} = \frac{e}{4\varepsilon_o}\sqrt{\frac{\alpha}{\Delta}} \tag{4.1}$$

Harland proposed the Δ will be equal to *IE* in case of gas phase of the target system. While, in the present case of aqueous phase species, the $\Delta = IE + E_{gap}$, and the ionization of the system actually occurs when the incoming energy is greater than the threshold value, $\Delta = IE + E_{gap}$.

Using this equation 4.1, we have predicted the α values for the present studied targets as given in the table 4.13.

Table 4.13 Predicted polarizability α (Å)³

Target	**Δ (eV)**	**$Q_{ion(m)}$ (Å)²**	**Predicted *α* (Å)³**	**Reference value for condensed phase (Å)³** [43]
Adenine	10.25	12.65	11.54	14.33
Guanine	9.60	15.47	16.17	15.26
Thymine	10.60	14.17	14.99	13.35
Cytosine	10.85	12.99	12.88	11.47
Uracil	11.25	11.32	10.15	10.41

From the table 4.13, it can be observed that the present predicted α for the aqueous molecules find good agreement with those of Nakagawa [43], who calculated the polarizability (α) for condensed molecules.

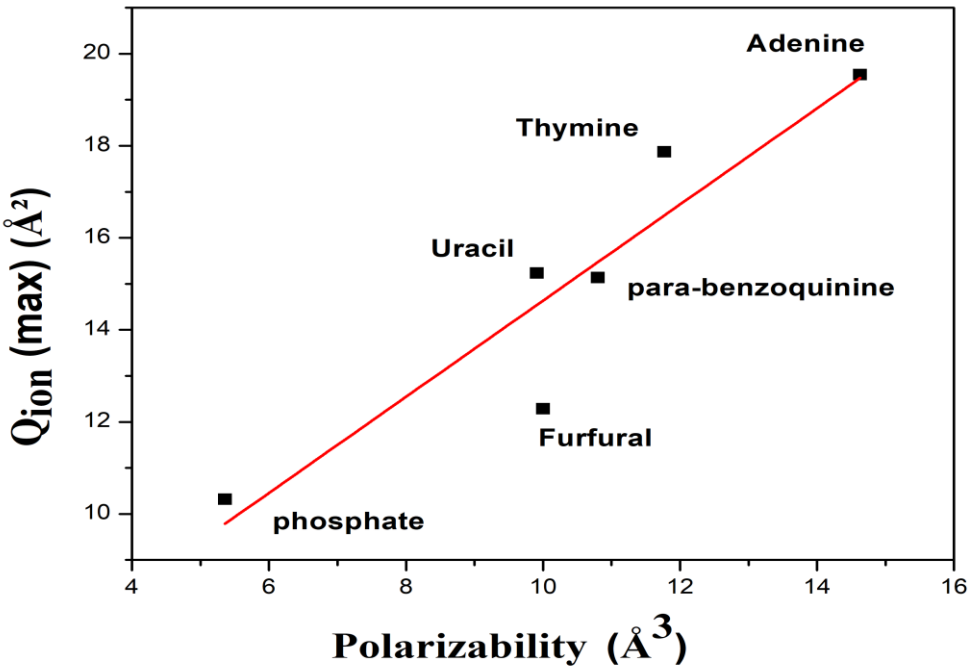

Figure 4.21 correlation between Q_{ion} (max) and dipole polarizability (α)

In figure 4.21, we can see linear correlation between $Q_{ion}(max)$ and polarizability. From this figure, we can forecast the value of polarizability with given Q_{ion} value.

4.5.3 Dielectric constant (ε):

The two expressions for dielectric constant (ε) have been derived in the present work using the dependency of the $Q_{ion(m)}$ on α and ε. The first proposed expression of dielectric constant as a function of $Q_{ion(m)}$, derived using the dependency of $Q_{ion(m)}$ with α (equation 4.1) and the Clausius-Mosotti (CM) equation,

$$\frac{\varepsilon-1}{\varepsilon+2} = C \cdot (Q_{ion}(max))^2 N\Delta \qquad (4.2)$$

Where, *C* is the constant = $\frac{64\pi}{3}\left(\frac{\varepsilon_o}{e}\right)^2$ and *N* is the number density of the molecule.

Secondly, the Onsager dielectric equation [44], which works well for the case of liquids is given by,

$$\frac{\varepsilon-1}{\varepsilon+2} = \frac{4\pi}{3}\alpha N + \frac{(\varepsilon-\varepsilon_\infty)(2\varepsilon+\varepsilon_\infty)}{\varepsilon(\varepsilon_\infty+2)^2} \quad (4.3)$$

This equation is thought to be more applicable in the present aqueous phase study, and again the equation of dielectric constant as a function of $Q_{ion(m)}$ is proposed as,

$$\frac{\varepsilon-1}{\varepsilon+2} = C \cdot \left(Q_{ion(m)}\right)^2 N\Delta + \frac{(\varepsilon-\varepsilon_\infty)(2\varepsilon+\varepsilon_\infty)}{\varepsilon(\varepsilon_\infty+2)^2} \quad (4.4)$$

Where, ε_∞ is the high frequency dielectric constant, which can be obtained from the CM equation. The computed ε values are listed in table 4.14.

Table 4.14 Computed dielectric constants (ε)

Target	**$Q_{ion(m)}$ (Å)²**	**Dielectric constant (ε) (Equation 4.1)**	**Dielectric constant (ε) (Equation 4.3)**	**Reference** [45]
Adenine	12.65	2.22	1.00	1.59
Guanine	15.47	3.23	0.85	1.77
Thymine	14.17	3.39	0.99	1.59
Cytosine	12.99	2.84	1.03	1.71
Uracil	11.32	2.29	0.98	-

Form the table 4.13, it can be observed as expected that the ε values computed through equation 4.3, are in good agreement with those of Szarek [45].

The dielectric constant for p-benzoquinone and furfural molecules has potential applications for the study of electrical energy storage device, pseudo capacitor, photo transistor, dye-

sensitized solar cells, artificial photosynthesis, rechargeable batteries, the evolution of new electronic devices and other electrical properties.

Relation between $Q_{ion}(max)$ and dielectric constant (ε)

The Clausius-Mossotti equation [46] yields,

$$\frac{\varepsilon-1}{\varepsilon+2} = \frac{4\pi}{3} * N * \alpha \quad (4.5)$$

According to Harland's proposed qualitative dependency nature of the $Q_{ion}(max)$ with its polarizability (α) using below equation (4.6).

Then we correlate this equation with dielectric constant (using Eq. 4.5),

$$Q_{ion}(max) = 11.92(\alpha) = 11.92\left(\frac{3*\left(\frac{\varepsilon-1}{\varepsilon+2}\right)}{4\pi N*IE}\right)^{0.5} \quad (4.6)$$

Using above-mentioned three methods, we have computed dielectric constant for present studied targets are shown in table 4.15. In table 4.15, we report number density and computed dielectric constant using polarizability for $C_5H_4O_2$ (Furfural) and $C_6H_4O_2$ (pBQ).

Table 4.15 Calculated Number density N and Dielectric constant ε

Mol.	$Q_{ion^{Max}}$ (Å²)	**α (10⁻²⁴ cm³)**	**ρ** g/cm^3	**M** g/mol	**N** cm^{-3}	**Dielectric constant (ε)**		
						C.M. [46]	**Onsager** [44]	[42]
$C_5H_4O_2$	12.283	10	1.16	96.1	$7.27x10^{21}$	2.31	0.99	1
$C_6H_4O_2$	15.134	10.8	1.32	108.1	$7.35x10^{21}$	2.49	1	1

In the case of Furfural, the relatively high dielectric constant is due to the polar nature of the molecule, which has a carbonyl group (C=O) and a furan ring that contains oxygen atoms. This property makes Furfural useful as a solvent for polar molecules and for use in various industrial applications that require a high dielectric constant.

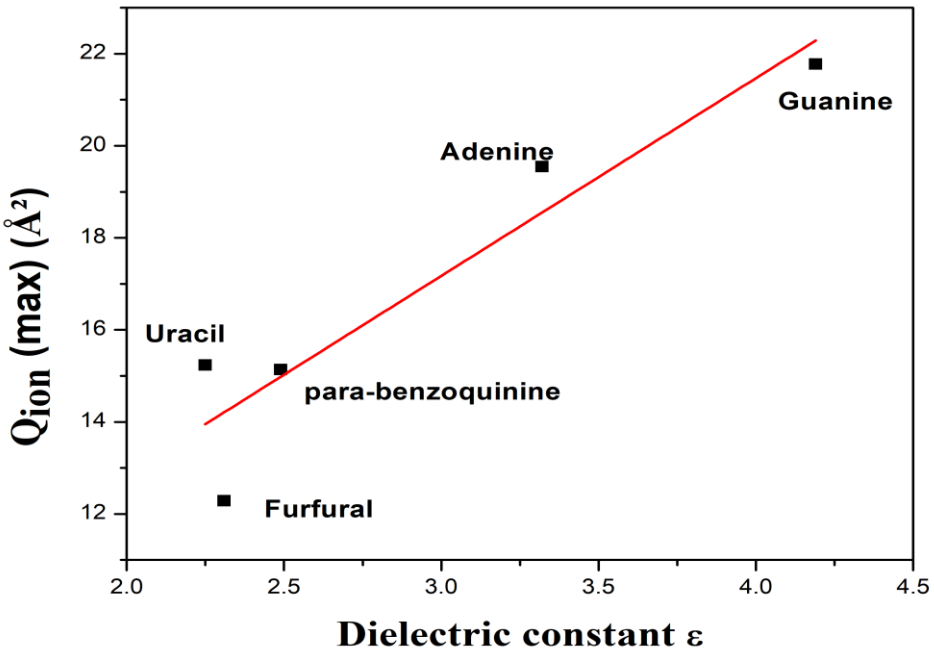

Figure 4.22 Correlation between $Q_{ion}(max)$ and dielecric constant (through Eq. 4.5)

From figure 4.22, we have observed linear relationship between maximum ionization cross section and dielectric constant from Clausius- Mossootti equation (4.5).

The Relatively low dielectric constant of parabenzoquinone is due to the non-polar nature of the molecule, which contains carbonyl groups but lacks polar functional groups such as hydroxyl or amino groups.

Prediction of polarizability and dielectric constant for PFPA

Table 4.16 shows various properties including polarizability and ionization Potential of $C_3F_5HO_2$ molecule. Table 4.16 display the estimated polarizability values, which have deviation of 20.97% from the actual value.

Table 4.16 Calculated and estimated dielectric constant (ε)

Target	Polarizability (α) ($10^{-24}cm^{-3}$)	Density of material (ρ) g/cm^3	Molar mass(M) g/mol	Calculated Number Density (N) $molecules/cm^3$	Estimated Dielectric constant (ε)	Calculated Dielectric Constant (ε)
$C_3F_5HO_2$	7.2	1.56	164.03	$5.7*10^{21}$	1.49	1.62

We have linear relationship between polarizability and dielectric constant from Clausius-Mossotti equation [46].

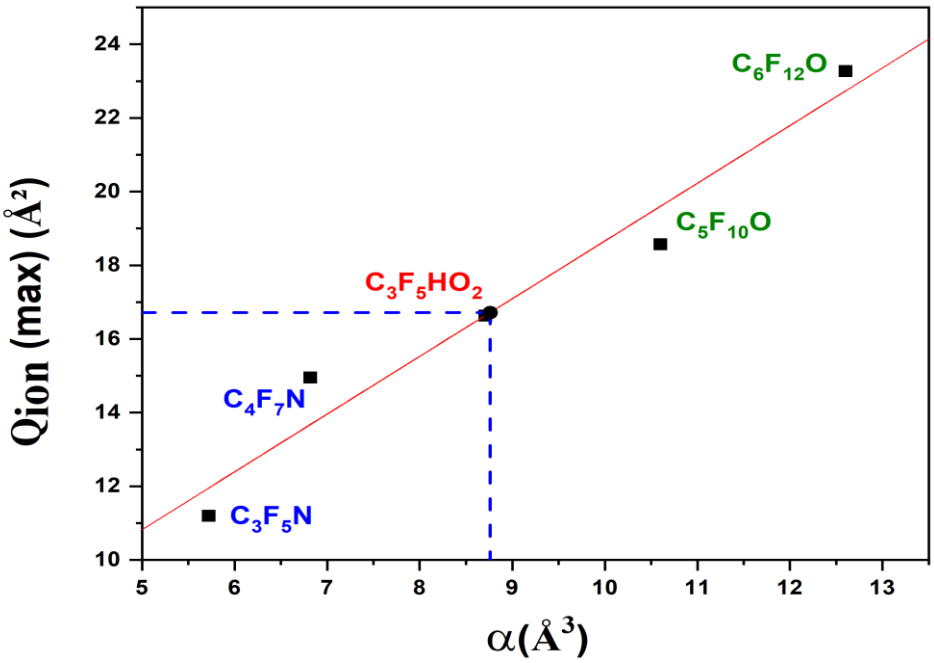

Figure 4.23 Variation of Q_{ion}(max) with α

It is possible to estimate the polarizability of given molecule by utilizing the linear correlation between Q_{ion}(max) and polarizability presented in figure 4.23.

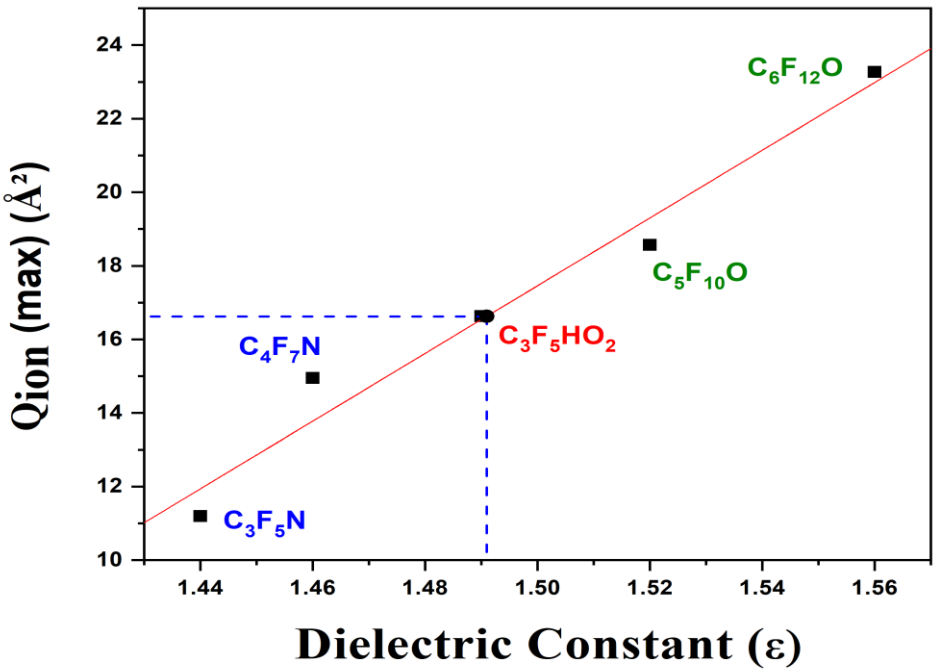

Figure 4.24 Variation of Q_{ion}(max) with ε

Figure 4.24 shows linear relation between dielectric constant and Q_{ion}(max).

4.6 Chapter Summary

In this chapter, the present work involves the quantification of the various interaction processes upon electron impact on to the aqueous DNA constituents. The present study has also analysed the dependency of the total cross-sections (Q_T) on the impact energy and molecular characteristics, followed by proposing a new approach, called 2-parameter semi-empirical method (2p-SEM) for estimating Q_T. This is the maiden attempt to report a single formula for Q_T, which is applicable for the larger and complex molecules with 55-95 electrons and for the energy range 50-5000 eV. Other than analysing the Q_T dependency, we have also studied the various correlations of maximum ionization cross-sections ($Q_{ion(m)}$) with the dielectric constant and molecular polarizability.

We have done exhaustive study on furfural and p-benzoquinone. Furfural has many potential uses in bio-fuel, pharmaceutical, agrochemical industries, etc. whereas; p-benzoquinone is an important molecule in energy storage device, pseudo battery, artificial photosynthesis, rechargeable batteries, the evolution of new electronic devices etc. For these applied molecules,

our cross sections data may be helpful in simulation. By using SCOP formalism, we quantified Q_T, Q_{el} and Q_{inel}, while Q_{ion} and ΣQ_{exc} were computed through CSP-ic method and compared with available results. A good agreement was noted between present total ionization (Q_{ion}) through CSP-ic with BEB and IAM-SCAR+I. We have used a 2p-SEM for energy range 50 to 5 keV. This formalism may be useful for estimation of Q_T, for those molecules/atoms whose experimental data are not available (especially due to experimental difficulties). In this paper we have tested this method for larger and complex molecules with target electrons $55 < Z < 95$. By examining the available total electron scattering cross sections for a number of various targets such as DNA constituent, we have observed that at intermediate to high energies the Q_T shows significant correlation with ground state target dipole polarizability. We also computed dielectric constant ε using Clausius-Mossotti, Onsager and by making use of molecular ionization cross sections. Further, we have observed several correlations, which may be helpful for the prediction of dipole polarizability and dielectric constant.

We reported quantified probabilities of various electron assisted molecular processes for $C_3F_5HO_2$ for wide impact energies (IP to 5 keV). We perform calculations for Q_{inel} and Q_{el} using the SCOP formalism and obtained Q_{ion} and ΣQ_{exc} through CSP-ic method and displayed results graphically in figures 4.19 and 4.20 For this applied molecule we also found number density N and reported dielectric constant ε using molecular polarizability. Thus, the current study of cross sections calculations upon electron impact can help to predict polarizability and dielectric constant for any materials of electrical applications.

4.7 Bibliography

[1] B. Boudaïffa, P. Cloutier, D. Hunting, M. A. Huels, and L. Sanche, *Cross Sections for Low-Energy (10-50 EV) Electron Damage to DNA*, Radiat Res **157**, 227 (2002).

[2] H. Nikjoo, R. Taleei, T. Liamsuwan, D. Liljequist, and D. Emfietzoglou, *Perspectives in Radiation Biophysics: From Radiation Track Structure Simulation to Mechanistic Models of DNA Damage and Repair*, Radiation Physics and Chemistry **128**, 3 (2016).

[3] D. T. Goodhead, *Initial Events in the Cellular Effects of Ionizing Radiations: Clustered Damage in DNA*, Int J Radiat Biol **65**, 7 (1994).

[4] L. Mozejko, Pawel; Sanche, *Cross Sections for Electron Scattering from Selected Components of DNA and RNA*, Radiation Physics and Chemistry **73**, 77 (2005).

[5] C. Bull, James N.; Lee, Jason W. L.; Vallance, *Absolute Electron Total Ionization Cross-Sections: Molecular Analogues of DNA and RNA Nucleobase and Sugar Constituents*, Physical Chemistry Chemical Physics **16**, 10743 (2014).

[6] B. Colyer, C. J.; Bellm, S. M.; Blanco F.; Garcia, G.; Lohmann, *Elastic Electron Scattering from the DNA Bases Cytosine and Thymine*, Phys Rev A (Coll Park) **84**, 042707 (2011).

[7] C. Mokrani, S; Aouchiche H.; Champion, *Elastic Scattering of Electrons by DNA Bases*, Radiation Physics and Chemistry **172**, 108735 (2020).

[8] M. Vinodkumar and C. Limbachiya, *Electron Impact Total and Ionization Cross-Sections for DNA Based Compounds*, Mol Phys **111**, 215 (2013).

[9] L. Toburen, *Ionization and Charge-Transfer: Basic Data for Track Structure Calculations*, Radiat Environ Biophys **37**, 221 (1998).

[10] A. Bass and L. Sanche, *Absolute and Effective Cross-Sections for Low-Energy Electron-Scattering Processes within Condensed Matter*, Radiat Environ Biophys **37**, 243 (1998).

[11] H. Khesbak, O. Savchuk, S. Tsushima, and K. Fahmy, *The Role of Water H-Bond Imbalances in B-DNA Substate Transitions and Peptide Recognition Revealed by Time-Resolved FTIR Spectroscopy*, J Am Chem Soc **133**, 5834 (2011).

[12] Helmholtz Association of German Research Centres, *Water Molecules Characterize the Structure of DNA Genetic Material.*, https://www.sciencedaily.com/releases/2011/04/110426091122.htm#citation_apa.

[13] Z. Tan, Y. Xia, X. Liu, M. Zhao, Y. Ji, F. Li, and B. Huang, *Cross Sections of Electron Inelastic Interactions in DNA*, Radiat Environ Biophys **43**, 173 (2004).

[14] P. de Vera, I. Abril, and R. Garcia-Molina, *Excitation and Ionisation Cross-Sections in Condensed-Phase Biomaterials by Electrons down to Very Low Energy: Application to Liquid Water and Genetic Building Blocks*, Physical Chemistry Chemical Physics **23**, 5079 (2021).

[15] H. Q. Tan, Z. Mi, and A. A. Bettiol, *Simple and Universal Model for Electron-Impact Ionization of Complex Biomolecules*, Phys Rev E **97**, 1 (2018).

[16] K. J. Zeitsch, *The Chemistry and Technology of Furfural and Its ManyBy-Products*, 1st ed. (Elsevier science, 2000).

[17] H. Kobayashi and A. Fukuoka, *Synthesis and Utilisation of Sugar Compounds Derived from Lignocellulosic Biomass*, Green Chemistry **15**, 1740 (2013).

[18] J.-S. H. Ajit Singh Mamman, Jong-Min Lee, Yeong-Cheol Kim, In Taek Hwang, No-Joong Park, Young Kyu Hwang, Jong-San Chang, *Furfural: Hemicellulose/Xylosederived Biochemical*, Biofuels, Bioproducts and Biorefining **2**, 438 (2008).

[19] and J. M. A. W. Khan, J.-P. Labrie, *Effect of Electron-Beam Irradiation Pretreatment on the Enzymatic Hydrolysis of Softwood*, Biotechnology Bioengineering **28**, (1986).

[20] M. A. R. Jayr Amorim, Carlos Oliveira, Jorge A. Souza-Corrêa, *Treatment of Sugarcane Bagasse Lignin Employing Atmospheric Pressure Microplasma Jet in Argon*, Plasma Processes and Polymers **10**, (2013).

[21] and M. A. P. L. M. A. Ridenti, J. A. Filho, M. J. Brunger, R. F. da Costa, M. T. do N. Varella, M. H. F. Bettega, *Electron Scattering by Biomass Molecular Fragments: Useful Data for Plasma Applications?*, The European Physical Journal D **70**, (2016).

[22] D. B. Jones, R. F. da Costa, M. T. D. N. Varella, M. H. F. Bettega, M. A. P. Lima, F. Blanco, G. García, and M. J. Brunger, *Integral Elastic, Electronic-State, Ionization, and*

Total Cross Sections for Electron Scattering with Furfural, Journal of Chemical Physics **144**, (2016).

[23] W. S. & P. O. Athina Zouni, Horst-Tobias Witt, Jan Kern, Petra Fromme, Norbert Krauss, *Crystal Structure of Photosystem II from Synechococcus Elongatus at 3.8 Å Resolution*, Nature **409**, 739 (2001).

[24] and T. A. M. M. Hambourger, G. F. Moore, D. M. Kramer, D. Gust, A. L. Moore, *Biology and Technology for Photochemical Fuel Production*, Chemical Society Review **38**, 25 (2009).

[25] and I. W. O. Yehezkeli, R. Tel-Vered, J. Wasserman, A. Trifonov, D. Michaeli, R. Nechushtai, *Integrated Photosystem II-Based Photo-Bioelectrochemical Cells*, Nat Commun **3**, 742 (2012).

[26] D. B. Jones, F. Blanco, G. García, R. F. Da Costa, F. Kossoski, M. T. D. N. Varella, M. H. F. Bettega, M. A. P. Lima, R. D. White, and M. J. Brunger, *Elastic Scattering and Vibrational Excitation for Electron Impact on Para -Benzoquinone*, Journal of Chemical Physics **147**, (2017).

[27] C. J. Zhang, Y. Qu, X. Zhao, and Q. Zhou, *Photoinduced Reductive Decomposition of Perflurooctanoic Acid in Water: Effect of Temperature and Ionic Strength*, Clean (Weinh) **43**, 223 (2015).

[28] C. A. Moody, J. W. Martin, W. C. Kwan, D. Muir, and S. Mabury, *Monitoring Perfluorinated Surfactants in Biota and Surface Water Samples Following an Accidental Release of Fire-Fighting Foam into Etobicoke Creek.*, Environ Sci Technol (2002).

[29] C. Zhang, H. Yan, F. Li, and Q. Zhou, *Occurrence and Fate of Perfluorinated Acids in Two Wastewater Treatment Plants in Shanghai, China*, Environ Sci Pollut Res Int **22**, 1804 (2015).

[30] J. W. Martin, S. A. Mabury, K. R. Solomon, and D. C. G. Muir, *Dietary Accumulation of Perfluorinated Acids in Juvenile Rainbow Trout (Oncorhynchus Mykiss)*, Environ Toxicol Chem **22**, 189 (2003).

[31] C. E. Crespo-Hernández, R. Arce, Y. Ishikawa, L. Gorb, J. Leszczynski, and D. M. Close, *Ab Initio Ionization Energy Thresholds of DNA and RNA Bases in Gas Phase and in Aqueous Solution*, Journal of Physical Chemistry A **108**, 6373 (2004).

[32] H. Fernando, G. A. Papadantonakis, N. S. Kim, and P. R. Lebreton, *Conduction-Band-Edge Ionization Thresholds of DNA Components in Aqueous Solution*, Proc Natl Acad Sci U S A **95**, 5550 (1998).

[33] S. Gop, R. Sutradhar, S. Chakraborty, and T. P. Sinha, *The Study of Energetic and Electronic Properties of Metal-Adenine Complex in Solvent Phase: A Density Functional Theory Approach*, in *AIP Conference Proceedings*, Vol. 2162 (American Institute of Physics Inc., 2019).

[34] M. T. Baei, M. R. Taghartapeh, E. T. Lemeski, and A. Soltani, *A Computational Study of Adenine, Uracil, and Cytosine Adsorption upon AlN and BN Nano-Cages*, Physica B Condens Matter **444**, 6 (2014).

[35] R. di Felice, A. Calzolari, E. Molinari, and A. Garbesi, *Ab Initio Study of Model Guanine Assemblies: The Role of (Formula Presented) Coupling and Band Transport*, Phys Rev B Condens Matter Mater Phys **65**, 1 (2002).

[36] J. MacNaughton, A. Moewes, and E. Z. Kurmaev, *Electronic Structure of the Nucleobases*, Journal of Physical Chemistry B **109**, 7749 (2005).

[37] A. Traoré Dubuis, A. Verkhovtsev, L. Ellis-Gibbings, K. Krupa, F. Blanco, D. B. Jones, M. J. Brunger, and G. García, *Total Cross Section of Furfural by Electron Impact: Experiment and Theory*, Journal of Chemical Physics **147**, (2017).

[38] A. I. Lozano, K. Krupa, F. Ferreira da Silva, P. Limão-Vieira, F. Blanco, A. Muñoz, D. B. Jones, M. J. Brunger, and G. García, *Low Energy Electron Transport in Furfural*, European Physical Journal D **71**, (2017).

[39] A. I. Lozano et al., *Total Electron Scattering Cross Sections from Para -Benzoquinone in the Energy Range 1-200 EV*, Physical Chemistry Chemical Physics **20**, 22368 (2018).

[40] D. B. Jones, R. F. da Costa, F. Kossoski, M. T. D. N. Varella, M. H. F. Bettega, G. García, F. Blanco, R. D. White, M. A. P. Lima, and M. J. Brunger, *Integral Elastic, Vibrational-Excitation, Electronic-State Excitation, Ionization, and Total Cross*

Sections for Electron Scattering from Para -Benzoquinone, Journal of Chemical Physics **148**, (2018).

[41] G. Garcıa and F. Maneró, *Correlation of the Total Cross Section for Electron Scattering by Molecules with 10-22 Electrons, and Some Molecular Parameters at Intermediate Energies*, Chem Phys Lett **280**, 419 (1997).

[42] P. W. Harland and C. Vallance, *Ionization Cross-Sections and Ionization Efficiency Curves from Polarizability Volumes and Ionization Potentials*, Int J Mass Spectrom Ion Process **171**, 173 (1997).

[43] S. Nakagawa, *Polarizable Model Potential Function for Nucleic Acid Bases*, J Comput Chem **28**, 1538 (2007).

[44] L. Onsager, *Electric Moments of Molecules in Liquids*, J Am Chem Soc **58**, 1486 (1936).

[45] P. Szarek, *Electric Permittivity in Individual Atomic and Molecular Systems Through Direct Associations with Electric Dipole Polarizability and Chemical Hardness*, Journal of Physical Chemistry C **121**, 12593 (2017).

[46] C. Kittel and D. F. Holcomb, *Introduction to Solid State Physics*, 8th ed., Vol. 35 (1967).